

ELECTRIC OCTOPOLE CONFIGURATIONS FOR FAST SEPARATION OF TRAPPED IONS

J. P. HOME

*Centre for Quantum Computation, Department of Atomic and Laser Physics, Clarendon Laboratory, Parks Road
 Oxford, OX1 3PU, England*

A. M. STEANE

*Centre for Quantum Computation, Department of Atomic and Laser Physics, Clarendon Laboratory, Parks Road
 Oxford, OX1 3PU, England*

Received (received date)

Revised (revised date)

We study the problem of designing electrode structures which allow pairs of ions to be brought together and separated rapidly in an array of linear Paul traps. We show that it is desirable for the electrode structure to produce a d.c. octopole moment with an a.c. radial quadrupole. For the case where electrical breakdown limits the voltages that can be applied, we show that the octopole is more demanding than the quadrupole when the characteristic distance scale of the structure is larger than 1 micron (for typical materials). We present a variety of approaches and optimizations of structures consisting of one to three layers of electrodes. The three-layer structures allow the fastest operation at given distance ρ from the trap centres to the nearest electrode surface, but when the total thickness w of the structure is constrained, leading to $w < \rho$, then two-layer structures may be preferable.

Keywords: Ion Trap, Multiple Traps

Communicated by: to be filled by the Editorial

1 Introduction

The application of ion traps to quantum computing has lead to interest in the construction of systems of multiple ion traps situated close together. Experiments have shown that quantum logic gates with good fidelity can be produced between a single pair of ions in a single trap, and such methods can be extended to a few ions in a single trap [1, 2, 3]. However, to scale this approach up to the manipulation of many qubits, it is not feasible to try to manipulate large numbers of qubits in a single trap. Instead, it is desirable to have an array of traps, with the possibility to move quantum information between ions in separate traps. A method to move the quantum information which has advantages of relative simplicity and robustness is simply to move the ions themselves [4, 5, 6]. To achieve this we need an array of ion traps, with the possibility to move ions between traps. This concept has been demonstrated in an impressive set of experiments [7, 8] which demonstrate its promise. The present work addresses the issue of how to build a basic element of such an array: a region in which a pair of ions can be brought together or separated rapidly, by adjusting d.c. voltages on electrodes. This includes the case of separating into two wells a pair of ions which are initially in a single harmonic well.

There are further constraints which make this a non-trivial problem:

- The electrode structure should allow a route for ions to be moved into and out of the region of the close pair of trapping centres.
- The surfaces of the electrodes should be kept as far as possible from the trap centres where the ions sit. This is in order both to minimise heating of the motional state of the trapped ions (see below) and to reduce the impact of surface irregularities on the electric potential function experienced by the ions.
- The trap confinement should be tight, i.e. the vibrational frequency ν of the ions must exceed some desired minimum value. This is in order to maximise the speed at which ions can be moved by displacing the trap centres.
- The electric fields at the electrode surfaces must not exceed the electrical breakdown limitations of the materials.
- The electrode configuration must be capable of being fabricated accurately at the required distance scale. This may require microfabrication techniques which have their own intrinsic limitations.

For diagnostic purposes it may also be useful for the electrode structure to be open in order to allow optical access.

The need to keep the electrode surfaces far away from the ions is largely owing to the observation of an anomalous heating rate in ion traps, which becomes a severe problem with traps of small distance scale. The heating process is not fully understood but appears to be associated with impurities deposited on the electrodes, and studies suggest the heating rate scales as ρ^{-4} where ρ is the distance from trap centre to the nearest electrode surface [9, 7, 10]. Electrodes further from the trap centre can also be bigger, which usually implies they are easier to make.

Typical distance scales are 1–10 microns for the separation of the trapped ions, 1–100 microns for the distance to the electrodes [9, 7, 8, 11].

We begin the discussion by considering in section 2 the general problem of a pair of 1-dimensional potential wells which can be moved together or pulled apart while maintaining the tightness, i.e. the normal mode frequencies of a pair of ions trapped in the wells. We argue that the best electrode structure is one which produces an electric octopole potential, which is then ‘tweaked’ by the addition of quadrupole terms. In section 3 we introduce radial confinement by an a.c. quadrupole, and discuss in general terms the expected scaling of the trap parameters with the size of the electrode structure. We show that for structures whose dimensions are greater than a few microns, the most demanding factor in the design is to obtain a large octopole moment, assuming the applied voltages are limited only by electrical breakdown of the materials. We then proceed in section 4 to consider the general problem of obtaining an electric octopole with a minimum number of electrodes. In section 5 we describe numerical calculations of the electric potential for several types of electrode structure, obtaining the values of two dimensionless factors that give the strength of the three-dimensional d.c. octopole and two-dimensional a.c. quadrupole moment at given breakdown field and trap scale.

Section 6 discusses the main features of the numerical results. For example, we quantify the relative merits of a 3-layer over a 2-layer or single-layer (planar) design. We estimate the impact of requiring the complete structure to be thin (to aid microfabrication). We present the main features of the behaviour when simple optimizations are introduced, such as adjusting the positions and relative sizes of electrodes. Section 7 concludes. The appendix gives some general information on simple charge distributions which produce electric octopoles.

2 Generic study of $V(x, y, z)$ for two traps close together

We consider first of all some general properties of the electric potential for two Paul traps located at $(x, y, z) = (0, 0, \pm s)$. We assume the vibrational frequencies $\omega_x, \omega_y, \omega_z$ of a single trapped ion are the same for the two traps. The precise relative sizes of ω_x, ω_y and ω_z are not crucial, but it will be useful if $\omega_x, \omega_y \gg \omega_z$. The electrode configurations to be discussed in later sections of the paper will produce the confinement along z primarily by d.c. voltages, and that along x and y primarily by an oscillating (r.f.) quadrupole field. However, we do not need to assume this for the general discussion in this section.

Let the distance from the origin to the nearest electrode surface be ρ . Since we aim to achieve close traps and far electrodes, we assume $s \ll \rho$. We can then usefully analyse the electric potential V near the origin by a Taylor or a multipole expansion. We further assume that the electrode construction is close to symmetric so that odd order terms in the expansion almost vanish. First let us consider V along the z axis:

$$V(0, 0, z) \simeq V_0 - E_0 z + \alpha z^2 + \beta z^4 \quad (1)$$

where we have dropped the cubic term since we assume that it is negligible. The signs of the coefficients E_0, α, β have been chosen so that E_0 is the electric field at the origin (assuming $dV/dx = dV/dy = 0$ there), and to create a double well potential we need $\alpha < 0$ and $\beta > 0$ (see figure 1).

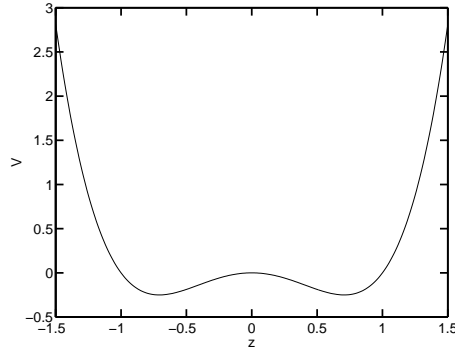


Fig. 1. Plot of $V(z)$ (equation (1)) for $V_0 = 0$, $E_0 = 0$, $\alpha = -1$, $\beta = 1$.

First suppose there is no linear term, $E_0 = 0$. By solving $\partial V / \partial z = 0$ we find for $\alpha < 0$ the potential wells are centred at

$$s = \sqrt{\frac{|\alpha|}{2\beta}}. \quad (2)$$

Evaluating $\partial^2 V / \partial z^2$ at either well centre gives $\partial^2 V / \partial z^2 = 4\alpha$. If the oscillating voltages are so arranged that the z axis is an r.f. null, i.e. $V(0, 0, z)$ is constant in time or only has a relatively small oscillation, then we may obtain ω_z for an ion trapped in either well directly from $\partial^2 V / \partial z^2$, giving

$$-\alpha = \frac{m\omega_z^2}{4q}, \quad (3)$$

where m, q are the mass and charge of the ion. For example, at $\omega_z / 2\pi = 1$ MHz, $|\alpha| \simeq 4$ MV/m² for the charge to mass ratio of the $^{43}\text{Ca}^+$ ion. The well depth $V(0) - V(s) = \alpha s^2 / 2$; e.g. 0.2 mV (2 Kelvin) at $s = 10$ μm .

In summary, the quadratic term α in the Taylor expansion sets the trap tightness (leading to ω_z), and the ratio of the quadratic to quartic terms sets the trap separation.

We will arrange for the linear term E_0 to be small by using electrodes symmetric under reflections in the $x-y$ plane, and then nulling any remaining field if necessary by compensation voltages. Let us calculate next the value of E_0 which “tips the potential over” just enough so that one of the traps cannot confine ions, i.e. $\partial^2 V / \partial z^2$ goes to zero at a trap centre. This happens when

$$|E_0| \simeq \frac{4}{3} |\alpha| s. \quad (4)$$

For example, for $^{43}\text{Ca}^+$ with $\omega / 2\pi = 1$ MHz and $s = 10$ μm , $|\alpha|s \simeq 40$ V/m.

2.1 *Cancellation of quadratic term*

Consider the Taylor expansion (1) for a set of electrodes of distance scale a . In the absence of special choices or symmetries which make one or more terms disappear, we would obtain

$$|E| \simeq \frac{|V_0|}{a}, \quad |\alpha| \simeq \frac{|V_0|}{a^2}, \quad |\beta| \simeq \frac{|V_0|}{a^4} \quad (5)$$

(for example, consider the electric potential due to a point charge, or a line charge, at distance a from the point or line). Therefore, without a special design, the order of magnitude of s is expected to be $s \sim a$. To obtain $s \ll a$ we require $\alpha/\beta \ll a^2$, and to obtain this without reducing ω_z we must increase β . This can be done by constructing an electrode configuration in which the quadratic term α is suppressed compared to β , and then increasing the voltages on all electrodes together. Assuming the increased voltages are attainable (and we will find they are), the available β at given α is limited by electrical breakdown associated with high electric fields at the electrode surfaces.

Assume that the electrodes have reflection symmetry in $x-y$, $x-z$ and $y-z$ planes, so that the electric field vanishes at the origin. Then odd-order multipole moments of $V(x, y, z)$ vanish, and so do mixed 2nd derivatives such as $\partial^2 V / \partial x \partial y$ at the origin. Under this assumption, we will next show that the required electrode configuration is one which produces, at lowest order in its multipole expansion around the origin, an octopole moment.

An electrode set that can produce $\alpha/\beta \ll a^2$ is close to the condition $\alpha \rightarrow 0$. Since we require the possibility to adjust α and β (e.g. by adjusting voltages on the electrodes) the same electrode set can also attain $\alpha = 0$ (in practice, it may or may not actually be used in that condition). We therefore have to consider electric potential configurations having $\partial^2 V / \partial z^2 = 0$

and $\partial^4 V / \partial z^4 \neq 0$. From Laplace's equation, we then have $\partial^2 V / \partial y^2 = -\partial^2 V / \partial x^2$, thus a 2D quadrupole moment in the $x - y$ plane unless these derivatives are also zero. Unless we take special measures to make $|\partial^2 V / \partial x^2|$ small, we have $|\partial^2 V / \partial x^2| \sim \beta a^2 \gg m\omega_z^2/q$ when $s \ll a$. This implies the field is strongly expelling along some direction in the $x - y$ plane. To permit the ions to remain trapped, either the whole field must be made to oscillate, or an oscillating quadrupole field must be added whose strength is sufficient to overcome this expulsion. If the whole field oscillates then in the pseudo-potential model, the effective values of both α and β are reduced, which is counter-productive. If instead a separate oscillating quadrupole is added in the $x - y$ plane (with small effect in the z -direction) then its strength must be large, and this leads to electrical breakdown which will constrain the available range of β .

We conclude that the d.c. electrode structure must be designed to produce small $|\partial^2 V / \partial x^2|$ (as well as small $|\partial^2 V / \partial z^2|$) and therefore we require an electrode structure at or close to an electric hexapole or octopole configuration. The octopole has the advantage that reflection symmetries which cancel odd-order multipole moments can be used to avoid producing an unwanted electric field (i.e. a contribution to the electric potential varying linearly with distance at the origin), and therefore we will concentrate on that case.

Confinement of the ions in three dimensions is completed by adding to the d.c. octopole field an oscillating 2D quadrupole field whose size is controlled separately. Hence, after reinstating a non-zero value for α , we obtain the general form

$$V(x, y, z, t) \simeq \alpha \left(z^2 - \frac{1}{2}(x^2 + y^2) \right) + \beta V_4(x, y, z) + Q_{ac} \cos(\Omega t)(x^2 - y^2) \quad (6)$$

where α , β and Q_{ac} are time-independent, $V_4(x, y, z)$ is an octopole potential with $V_4(0, 0, z) = z^4$, and Ω is the frequency of the a.c. quadrupole providing confinement in the radial direction. Many ion trap configurations in common use are described by (6), but we have in mind a case where $\beta/|\alpha|$ is as large as possible. We will see later that none of the electrode sets to be discussed realise (6) exactly, because the time-dependent part depends slightly on z as well as x and y , and because higher-order terms appear, but it is useful to make clear what we are aiming at.

2.2 Coulomb repulsion and normal mode frequencies

If there is one ion in each trap, then the distance between ions is not $2s$ owing to their mutual Coulomb repulsion. The equilibrium positions are $z = \pm s\xi$ where ξ is a real positive solution of

$$\xi^5 + \frac{\alpha}{|\alpha|} \xi^3 = \epsilon, \quad (7)$$

where

$$\epsilon = \frac{q}{4\pi\epsilon_0|\alpha|(2s)^3}. \quad (8)$$

For large ϵ (i.e. small $|\alpha|$ and s , a pair of close traps) the solution is $\xi \simeq \epsilon^{1/5}$. For small ϵ and $\alpha > 0$, i.e. two ions in the same harmonic well, the solution is $\xi \simeq \epsilon^{1/3}$. For small ϵ and $\alpha < 0$, i.e. a pair of well-separated traps, the solution is $\xi \simeq 1 + \epsilon/2$.

The system of two ions has two normal modes for motion along the z direction: the centre of mass mode of frequency ω_1 and the breathing (also called stretch) mode of frequency ω_2 . These frequencies are given by

$$\omega_1^2 = (2\alpha + 3\beta d^2) q/m, \quad (9)$$

$$\omega_2^2 = \omega_1^2 (1 + \tilde{\epsilon}), \quad (10)$$

where

$$\tilde{\epsilon} = \frac{q^2}{\pi\epsilon_0 m \omega_1^2 d^3} \quad (11)$$

and $d(\alpha, \beta) = 2\xi s$ is the equilibrium separation of the ions (m was defined previously, it is the mass of a single ion).

When the ions are far apart, $\tilde{\epsilon} \rightarrow \epsilon$ and the two mode frequencies are both equal to the oscillation frequency of a single ion in either trap. When $\alpha = 0$, $\tilde{\epsilon} = 2/3$ and when $\alpha \gg 1$ (i.e. a single harmonic well), $\tilde{\epsilon} \rightarrow 2$.

The reason to bring the ions close together is in order to perform a two-ion quantum logic gate in which their Coulomb repulsion provides the interaction energy between the qubits. The gate is fast when the mode frequencies are high and well-separated [12, 13]. Therefore we would like a high value of both ω_1 and $\tilde{\epsilon}$. Suppose the ions are initially in traps far apart, so that $\tilde{\epsilon} \ll 1$. Then the vibrational frequencies are almost equal and are given by the value of α through eq. (3). To bring the ions together, the voltages on the electrodes may be changed so that β gets larger while α stays the same size. Eventually electrical breakdown prevents further increase of β . If at this point the values of ω_1 and $\tilde{\epsilon}$ are high enough to give an acceptable gate speed, and if it possible to apply the logic-gate laser pulses to ions in the separation zone, then the gate is performed and the ions are subsequently separated. Otherwise, to bring the ions into a common trap, $|\alpha|$ must be lowered and one accepts an unavoidable reduction in mode frequencies while the potential barrier between the twin traps is lowered. After α passes through zero and becomes positive, the mode frequencies increase again and $\tilde{\epsilon}$ rises towards its maximum value of 2. The ions can then be moved as a pair to a convenient (e.g. less noisy) region of the complete array, for the logic-gate laser pulses to be applied.

At the condition $\alpha = 0$, the full analysis is tractable and one finds

$$\omega_1 = \sqrt{\frac{3q}{m}} \left(\frac{q}{2\pi\epsilon_0} \right)^{1/5} \beta^{3/10} \quad (12)$$

and $\tilde{\epsilon} = 2/3$ as mentioned above.

In the rest of this paper we will consider methods to produce this condition, i.e. an octopole potential, with an added oscillating quadrupole potential in the $x - y$ plane, as in (6).

3 Radial r.f. confinement and scaling

Consider the potential (6). A pair of trapped ions is confined in the radial (x and y) direction by the oscillating quadrupole field. To first approximation we may ignore the effect

of the octopole potential on the radial motion, then this motion is described by a Mathieu equation. In the pseudo-potential model, for $\alpha = 0$, the secular frequency of the centre-of-mass vibrational motion in the radial direction is given by [14, 15]

$$\omega_r = q_r \Omega / 2\sqrt{2}, \quad (13)$$

where

$$q_r = \frac{4qQ_{ac}}{\Omega^2 m} \quad (14)$$

is the Mathieu q -parameter. For stable motion, q_r must not be large; values in the range 0.1 to 0.5 are typical. This constrains the applied r.f. frequency Ω and hence we obtain

$$\omega_r = \left(\frac{q_r q}{2m} Q_{ac} \right)^{1/2}. \quad (15)$$

At the octopole condition, equations (12) and (15) give the centre of mass vibrational frequencies for motion in the axial and radial directions respectively. Since we want the ions to align themselves along the z axis, we require $\omega_r > \omega_1$ (and $\omega_r \gg \omega_1$ is desirable). This sets a lower limit on the required value of Q_{ac} for given β :

$$Q_{ac} \geq \frac{6}{q_r} \left(\frac{q}{2\pi\epsilon_0} \right)^{2/5} \beta^{3/5}. \quad (16)$$

It is useful to examine the way these parameters scale with ρ , the distance from the origin to the nearest electrode structure, and E_{\max} , the largest electric field at an electrode surface. For a given electrode geometry ρ sets the distance scale of the electrodes. To keep E_{\max} as small as possible, the electrode surfaces should have as large a radius of curvature as possible, and therefore their radii should be allowed to increase with ρ . In other words the complete structure of the electrodes is assumed to scale with ρ . Nevertheless for a given electrode set at a given value of E_{\max} , β and Q_{ac} still have a range of possible values, because it is possible to choose a range of values for the ratio between the sizes of the oscillating and the d.c. voltages. Typically the variation is such that there is a competition between high β and high Q_{ac} .

In order to obtain the main features by a relatively simple analysis, we define two geometric factors γ and μ such that

$$\text{for } Q_{ac} = 0, \quad \beta = \frac{\gamma E_{\max}}{\rho^3}, \quad (17)$$

$$\text{for } \beta = 0, \quad Q_{ac} = \frac{\mu E_{\max}}{\rho}. \quad (18)$$

Thus γ and μ tell us about the maximum values of β and Q_{ac} available for a given electrode geometry, but we keep in mind that it is not possible to have both these maximum values at once.

Suppose the ions each have one electronic unit of charge and let A be the mass number, then for a trap at the octopole condition ($\alpha = 0$), eq. (12) gives

$$\frac{\omega_1}{2\pi} [\text{MHz}] \simeq \frac{840}{\sqrt{A}} \frac{(\gamma E_{\max})^{3/10}}{\rho^{9/10}}. \quad (19)$$

where E_{\max} is in V/ μm and ρ is in μm . Note that this mode frequency scales almost linearly with $1/\rho$, and is relatively insensitive to γ and E_{\max} . The radial frequency (eq. (15)), on the other hand, scales as

$$\omega_r \propto \frac{\mu^{1/2}}{\rho^{1/2}}. \quad (20)$$

Since ω_1 grows more rapidly than ω_r as the distance scale ρ is reduced, it follows that the condition $\omega_r > \omega_1$ can only be met at small ρ if the trap is operated with β below its maximum possible value. To avoid too great a reduction we need to make ω_r as high as possible and therefore μ gives the main limit on the performance. At large ρ , on the other hand, the condition $\omega_r > \omega_1$ is readily met and we can operate with β close to its maximum value, so then γ gives the main limit on the performance.

Figure 2 shows the frequencies ω_1 (eq. (19)) and ω_r (eq. (15)) plotted as a function of ρ for two example electrode configurations discussed in section 5. In order that a single graph can show the behaviour for all ion species, the vibrational frequencies are shown in units of a basic frequency ω_0 which depends on the charge/mass ratio of the ion. We define ω_0 to be the radial secular frequency (eq. (15)) for an ion in a trap having $Q_{\text{ac}} = 10^6 \text{ Vm}^{-2}$ and $q_r = 0.3$. $\omega_0/2\pi$ takes the value 92.3 kHz for $^{43}\text{Ca}^+$, 57.4 kHz for $^{111}\text{Cd}^+$ and 201.7 kHz for $^9\text{Be}^+$.

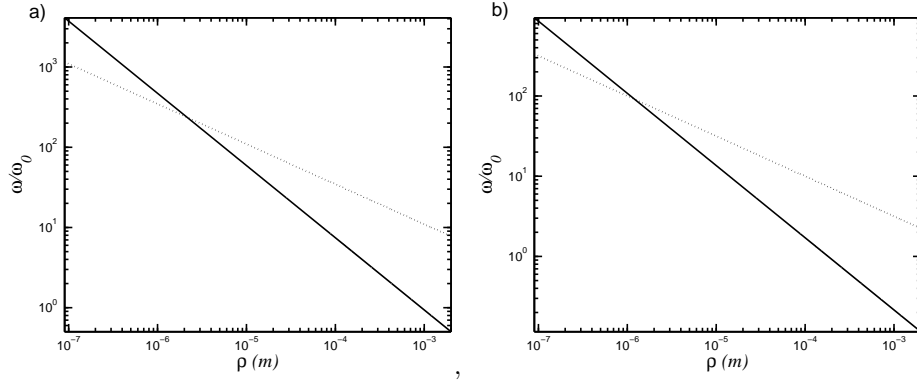


Fig. 2. Centre-of-mass vibrational frequencies for axial motion of two ions in a d.c. octopole potential (solid line, ω_1) and radial motion of two ions in a linear Paul trap (dashed line, ω_r). The frequency unit ω_0 is defined in the text. (a): electrode arrangement 2.1, (b): electrode arrangement 5.1. The frequencies are obtained using values of γ and μ presented in section 5 and using $E_{\max} = 10^6 \text{ V/m}$.

In order to find the distance scale ρ_c when the transition from large to small ρ takes place, we substitute (17) and (18) into (16). This gives a condition on γ and μ that can be expressed as a condition on the distance scale:

$$\rho_c \equiv \left(\frac{\gamma^3}{\mu^5} \right)^{1/4} \left(\frac{6}{q_r} \right)^{5/4} L_0 \quad (21)$$

where

$$L_0 = (q/2\pi\epsilon_0 E_{\max})^{1/2}. \quad (22)$$

L_0 is a fundamental distance scale set by the maximum electric field allowed by the materials. For example when $E_{\max} = 10$ MV/cm (the order of magnitude when field emission may occur [16, 17]), $L_0 \simeq 1.7$ nm. The factor $(6/q_r)^{5/4} \simeq 50$ to 100 for a reasonable choice of the Mathieu parameter. We thus find that for a wide range of values of γ and μ (with $\gamma < \mu$) the transition distance scale ρ_c is of the order of 0.1 to 1 μm . For electrodes structures larger than this, the chief difficulty is to obtain a large d.c. octopole moment; for electrode structures smaller than this, the chief difficulty is to obtain a large a.c. quadrupole moment.

Another interesting distance related to L_0 is the distance between the ions when the electrodes are close to the octopole configuration. This is given by $d_8 = 2\xi s$ with $\xi = \epsilon^{1/5}$, from which we obtain

$$d_8 = \rho \left(\frac{L_0^2}{\gamma \rho^2} \right)^{1/5}. \quad (23)$$

Therefore $d_8 \ll \rho$ when $\rho \gg L_0/\gamma^{1/2}$. This is usually the case. Therefore when the electric potential is just at the point of producing a potential hill between the ions, the distance between them is much smaller than the distance to the electrodes. This implies that the Taylor expansion we have adopted is valid.

4 Realising Octopoles

In this section we discuss general methods to obtain an octopole moment at the origin of coordinates. This acts as a guide in the design of the electrodes.

Three examples of octopole potentials are the axially symmetric octopole:

$$V = z^4 - 3z^2(x^2 + y^2) + \frac{3}{8}(x^2 + y^2)^2 \quad (24)$$

an octopole with cubic symmetry:

$$V = x^4 + y^4 + z^4 - 3(x^2y^2 + x^2z^2 + y^2z^2) \quad (25)$$

and the 2-dimensional octopole in the x - z plane:

$$V = z^4 + x^4 - 6z^2x^2. \quad (26)$$

The axially symmetric octopole can be produced by a set of 2 (+ve) end-cap and 3 ring (2 -ve, central one +ve) electrodes, all shaped to follow contours of V . The 2D octopole can be produced by a set of 8 (4 +ve, 4 -ve) rod electrodes parallel to the y axis and located at the corners of an octagon. These two examples of pure octopoles give a useful pointer to the required distribution of image charge.

The methods and image charge distributions listed below do not produce pure octopoles, but have an octopole as the leading term in the multipole expansion of their potential near the origin.

4.1 Use of symmetry

To produce an octopole at a point r , 19 constraints have to be satisfied. These are that the first, second and third derivatives of the potential at this point in three orthogonal directions

should vanish. Many of these can be satisfied by the introduction of symmetry to the charge distribution producing the potential. This can take the form of either rotation symmetry about an axis passing through \underline{r} , or reflection symmetry in a plane containing the point \underline{r} .

A single reflection in a plane containing the point \underline{r} produces zero odd-order moments in a direction perpendicular to the plane, and also forces the mixed second derivatives such as $\partial^2 V / \partial x_i \partial x_j$ to vanish, where x_i lies within and x_j lies perpendicular to the plane of reflection. This leaves 12 constraints to be satisfied.

Two reflections in orthogonal planes containing \underline{r} produces zero odd-order moments in the directions normal to the two planes, and all mixed second derivatives vanish. This leaves 7 constraints to be satisfied.

Two-fold rotation symmetry about an axis passing through \underline{r} causes the odd-order derivatives of the potential in all directions perpendicular to the axis to vanish, reducing the number of constraints to 9.

Four-fold rotation symmetry about an axis passing through \underline{r} makes the second derivatives in directions perpendicular to the axis equal, hence the number of constraints is reduced to 5.

Combinations of the above can be used to reduce the number of constraints further. Reflection symmetry in three orthogonal planes all containing \underline{r} reduces the constraints to 3, on the non-mixed second derivatives $\partial^2 V / \partial x_i^2$. Combining a two-fold rotation about an axis passing through \underline{r} with a reflection in a plane normal to the axis and containing \underline{r} reduces the constraints to 4 (the non-mixed second derivatives and the derivative $\partial^2 V / \partial x_i \partial x_j$, where x_i and x_j are orthogonal directions perpendicular to the rotation axis). A four-fold rotation symmetry about an axis passing through \underline{r} combined with a reflection in a plane normal to the axis and containing \underline{r} leaves 2 constraints (on the three non-mixed second derivatives, two of which are equal).

Finally, Laplace's equation reduces the degrees of freedom of the non-mixed second derivatives $\partial^2 V / \partial x_i^2$ by one.

4.2 *Image charge constructions*

(A). An octopole with cubic symmetry is produced by any arrangement of charge having cubic symmetry. Proof: the symmetries under reflections in three orthogonal planes imply the odd-order multipole moments vanish, and so do mixed second derivatives of V such as $\partial^2 V / \partial x \partial y$; the symmetries under rotation through 90° imply the coefficients of x^2 , y^2 and z^2 in a Taylor expansion of the potential at the centre of symmetry are all the same, and therefore by Laplace's equation they all vanish.

(B). An octopole with cylindrical symmetry is produced by any arrangement of charge having cylindrical symmetry, reflection symmetry in $z = 0$, and placed such that $\partial^2 V / \partial z^2 = 0$ (where z is the symmetry axis). Proof: the second derivatives w.r.t. x and y must be equal by symmetry and therefore by Laplace's equation they also vanish.

(C). An octopole is produced by any arrangement of charge having four-fold rotational symmetry in the $x-z$ plane, reflection symmetry in $y = 0$, and arranged so that $\partial^2 V / \partial y^2 = 0$. The reasoning is the same as in the previous case. The resulting octopole potential is a combination of the axially symmetric case (24) and the 2-dimensional case (26) oriented such that y is the common axis.

(D). An octopole can be produced, starting with any arrangement of charge $\rho(x, y, z)$, by the following recipe. First ensure reflection symmetries in order to cancel odd multipole moments, by forming

$$\bar{\rho} \equiv \sum_{i=0}^1 \sum_{j=0}^1 \sum_{k=0}^1 \rho((-1)^i x, (-1)^j y, (-1)^k z). \quad (27)$$

Next, form

$$\bar{\rho}' \equiv \bar{\rho}(x, y, z) - \bar{\rho}(x/f, y/f, z/f). \quad (28)$$

where $f \neq 1$ is a numerical factor. $\bar{\rho}'$ produces an octopole at the centre of symmetry. This can be proved by evaluation of the second derivatives of $V(\mathbf{r}) \propto \int \bar{\rho}'(\mathbf{r}')/|\mathbf{r} - \mathbf{r}'| d\tau$ at the origin. A proof giving further physical insight is as follows. $\bar{\rho}(x/f, y/f, z/f)$ produces the same functional form of $V(x, y, z)$ as $\bar{\rho}(x, y, z)$ but on a distance scale expanded by a factor f . Modelling $\bar{\rho}$ as a set of point charges, each charge in the rescaled distribution is now further from the origin by a factor f , and is increased in size by a factor f^3 . Since the second derivatives of V due to a point charge go as (distance) $^{-3}$, it follows that the second derivatives of the new potential are equal and opposite to those of the original one, QED. The fourth derivatives scale as (distance) $^{-5}$, so

$$\frac{\partial^4 \bar{V}'}{\partial x_i^4} = \left(1 - \frac{1}{f^2}\right) \frac{\partial^4 \bar{V}}{\partial x_i^4}. \quad (29)$$

where \bar{V}' (\bar{V}) is the potential due to $\bar{\rho}'$ ($\bar{\rho}$) respectively.

A natural extension of this method can produce higher order multipole configurations.

(E). An octopole can be formed by taking almost any charge distribution $\rho(x, y, z)$, and displacing and reflecting it in three dimensions. A general displacement to $\rho(x - x_0, y - y_0, z - z_0)$ has three free parameters (x_0, y_0, z_0) . One can be absorbed into an overall scale factor, leaving two. This is just enough free parameters to allow the two constraints

$$\begin{aligned} \frac{\partial^2 V}{\partial x^2}(0, 0, 0) &= 0 \\ \frac{\partial^2 V}{\partial y^2}(0, 0, 0) &= 0 \end{aligned} \quad (30)$$

to be satisfied, where V is the potential due to $\rho(x - x_0, y - y_0, z - z_0)$, except in rare cases when the form of ρ leads to no solution. The nulling of $\partial^2 V / \partial z^2$ follows from Laplace's equation. Finally, introduce reflection symmetry as in (27), which causes odd-order moments and mixed second derivatives ($\partial^2 V / \partial x \partial y$ etc.) to vanish.

Another way to understand this construction is to argue that most charge distributions produce a potential with zero second derivatives with respect to fixed orthogonal axes at some point in space; it suffices to place the origin at such a point and then introduce reflection symmetry. For example, if ρ corresponds to a single point charge, this construction leads to point charges on the corners of a cube. More generally if $\rho(x, y, z)$ lies in the x - z plane, this construction leads to a distribution of charge in two parallel planes at $y = \pm y_0$.

(F). All the above constructions involve constraints on the locations of the image charges in addition to the basic assumption of three-fold reflection symmetry. Our next construction

does not. An octopole can always be formed (with rare exceptions arising in pathological cases) by a charge distribution $\bar{\rho}$ with reflection symmetry as in (27), based on

$$\rho(x, y, z) = \rho_0 + f_1\rho_1 + f_2\rho_2 \quad (31)$$

where $\rho_i(x, y, z)$ ($i = 0, 1, 2$) are three different charge distributions located anywhere in the positive octant, and f_1 and f_2 are parameters whose values are given by solving the simultaneous equations

$$\left. \begin{aligned} \frac{\partial^2 V_0}{\partial x^2} + f_1 \frac{\partial^2 V_1}{\partial x^2} + f_2 \frac{\partial^2 V_2}{\partial x^2} &= 0 \\ \frac{\partial^2 V_0}{\partial z^2} + f_1 \frac{\partial^2 V_1}{\partial z^2} + f_2 \frac{\partial^2 V_2}{\partial z^2} &= 0 \end{aligned} \right\} \quad (32)$$

(evaluated at the origin), in which V_i are the potentials due to ρ_i . This construction uses the same property invoked in the previous one, namely that after cancellation of odd-order moments there are only two constraints (30) we need to satisfy. This implies that we only need two free parameters, and these are provided by f_1 and f_2 .

(G). When we abandon a reflection symmetry, the octopole can be regained by inserting further charges. For example, suppose we only have reflection symmetry in the x - y and y - z planes. This is the case, for example, when all the charges are located in or on a single substrate, with the octopole centred above the top surface of the substrate. Then in addition to (30) we have 4 further constraints, on V_y , V_{yyy} , V_{xxy} , V_{zzy} . One or more of these can be satisfied by a careful placement of a single charge distribution. Alternatively, charges are placed at any convenient position, and then their magnitudes are adjusted, similar to construction (F). To obtain the desired behaviour of the trapping centres, we don't need to insist on an octopole, however. Of these further constraints, only $V_y = 0$ is strictly necessary.

4.3 *Application to electrode design*

The distributions of charge discussed above are to be realised on the surfaces of a set of conducting electrodes at fixed voltages (or else they are image charge distributions which lead to the same equipotential surfaces). We wish to avoid complicated electrode shapes so we restrict ourselves to electrodes approximating to simple combinations of lines, rings, or sheets.

In order to satisfy N constraints on derivatives of $V(x, y, z)$ merely by adjusting voltages on electrodes, it is necessary to have $N + 2$ electrodes, since one defines a voltage zero, and the next one sets an overall scale factor. In order to produce radial confinement, a set of r.f. electrodes is introduced around (or in between) the d.c. ones which create the octopole. These r.f. electrodes also serve to define the d.c. zero. Thus, in construction (F) we require one r.f. voltage at d.c. ground, and 3 adjustable d.c. voltages; in construction (G) we require one r.f. voltage at d.c. ground, and 7 adjustable d.c. voltages.

Most of the constructions presented in the previous section can be ruled out, as follows.

The case of cubic symmetry (A) involves 8 electrodes, but to preserve precise symmetry these would have to lie along the edges or the extended major diagonals of a cube, which is difficult to fabricate, and a linear r.f. electrode set would also break the symmetry.

Case (B) can be realised with just two ring-shaped electrodes. This involves the fewest electrodes. For a Penning trap one would choose the magnetic field direction as the axis of symmetry of the rings. For a Paul trap the need to provide an additional r.f. quadrupole producing radial confinement in the $x - y$ plane suggests that there will be further electrodes

parallel to the z axis. This implies the fabrication is more straightforward if the rings are placed around another axis, which we take to be the y axis, so that all the electrodes lie in a set of parallel planes. The r.f. electrodes then destroy the circular symmetry. To regain a simple design, the rings can be replaced with rectangular loops, c.f. construction (C).

The other cases can all be fabricated in layers. The method of (28) (case (D)) involves up to 16 electrodes in total or 8 if they all lie in a plane; the method by displacement (case (E)) involves 8 electrodes in two parallel planes, the method of (31) (case (F)) involves up to 24 electrodes in general, or up to 12 if they all lie in a plane, which we take to be the $x - z$ plane. This can be reduced to 10 if one pair lies on the x axis. We avoid placing electrodes along the z axis, because we want to be able to bring ions into and out of the structure by moving them along this axis.

The minimal number of electrodes for a perfectly constructed system is not the only consideration, however. Manufacturing imprecision, patch potentials, and the desire to adjust the trap separation all imply that further electrodes will be needed to trim the system. The electrode structures which rely on precise construction to produce an octopole (cases (A)-(E)) require more of these extra electrodes than those which depend on variable voltages (cases (F) and (G)).

Screening effects arise when we consider conducting electrodes rather than merely charge distributions. The innermost electrodes tend to act like a Faraday cage to modify and screen the effects of the outer ones. Let P be the centre of the region in which we require a certain potential form (here, P is at the origin). A rough rule of thumb is that if there is not an unobscured line of sight from P to a given electrode, then the influence of that electrode on the potential at or near P is greatly modified by the obstructing electrode. However, the outer charge distribution in (28) is, by construction, exactly on an extended line from the origin to the inner charge distribution. Therefore an electrode set built with the aim of realising the recipe (D) suffers from screening effects and it is difficult to obtain a surface charge distribution of the form (28).

In the remainder of this paper we will concentrate on the case (F) of 10 electrodes all in the $x-z$ plane, of which one pair lies along the x axis, the case (E) of 8 or more electrodes in two planes at $y = \pm y_0$, and the case (G) of an octopole situated above all the electrodes. For the sake of completeness, the appendix lists some other examples of octopoles based on simple distributions of point, line and ring charges.

5 Optimization of some example structures

In this section we study various electrode arrangements and obtain the geometric factors γ (eq. (17)) and μ (eq. (18)) in each case. We optimize the most promising designs by adjusting electrode positions and relative sizes in order to maximise both factors.

In all the configurations to be discussed, we choose the z axis along the line where the twin traps are situated, the $x - z$ plane is parallel to the planes containing sets of electrodes, and hence these planes are separated along the y -direction.

To calculate a value for the parameter $\gamma = \rho^3 \beta / E_{\max}$, we numerically solve Laplace's equation for each electrode set-up, obtaining $\beta = (1/24) \partial^4 V / \partial z^4$ evaluated at the origin, and E_{\max} by examining the gradient of V near the surfaces of all the electrodes. Typically γ is a function of the relative positions and sizes of the electrodes; we search for the largest γ in

each case.

In order to calculate μ , calculations were performed with the r.f. electrodes at a voltage of 10^6V which is large compared to d.c. voltages of $\sim 1\text{V}$ used for the d.c. electrodes. The value of the radial confinement α_r was extracted, along with the value of the maximum field E_{max}^μ at the surface of the electrodes. The radial geometrical parameter μ was then calculated using equation (18). This parameter was calculated along the principal axes of the quadrupole perpendicular to the z axis. In most cases these were the x and y directions (giving μ_x and μ_y). Where this is not the case the radial geometrical parameters are denoted by $\mu_{x'}$ and $\mu_{y'}$. Where μ_x and μ_y differ, a component of the oscillating quadrupole potential lies along z , hence a trapped ion would experience a pseudopotential which would confine it along the z axis. As long as $|\mu_x - \mu_y|$ is not too large, this contribution has only a minor effect on the process of separation or bringing together of a pair of ions, merely shifting the value of α at which the ions experience a flat pseudopotential along z .

The numerical electric potential calculations were performed using Simion [18] and CPO [19]. Simion uses a finite difference method to find the potential of a regular 3D array of points. The array is iteratively relaxed so as to satisfy Laplace's equation and the boundary conditions, until the fractional changes per iteration were all below 5×10^{-3} . However, from simulations of analytically solvable cases, we found that the error in electric fields close to spherical and cylindrical electrodes could be as high as 10%. CPO uses a surface charge method, and we found it to be considerably faster and also much more precise. All the results presented here were obtained using CPO.

Since the numerical methods are slow, we first gained some general insights by analytic methods. We roughly modelled the electrodes as a set of line charges, and wrote down the complete potential function. This permits γ to be found as a function of various parameters, such as the line charges and their positions, and it can be maximised analytically. Results from such analyses gave a starting point for the electrode structures used in the numerical studies.

In order to know what value of γ and μ one might hope for, we numerically calculated these parameters for two simple cases. These can be regarded as a 'standard' against which the results for our various electrode structures can be measured. As a standard for μ , we used four cylindrical electrodes of radius $0.41254a$ with axes aligned along the z axis, and centred at the corners of a square of side $2a$. This arrangement gave $\mu = 0.20$. Electrodes of radius $0.3a$ centred at the same positions gave $\mu = 0.15$.

To obtain a standard value for γ , an electrode structure loosely based on the equipotentials of the axially symmetric octopole in equation 24 was used. This consisted of three toroidal electrodes centred on the z axis at $z = 0$ and $z = \pm 0.643a$, with two spherical "end-cap" electrodes of radius $0.35a$ at $z = \pm a$. The cross-section radii of the torii tubes and the radii of the centres of the tubes were $0.2a$ and a respectively for the $z = 0$ torus and $0.2a$ and $0.766a$ respectively for the $z = \pm 0.643a$ torii. This configuration gave $\gamma = 0.133$.

5.1 8 d.c. electrodes in 2 planes, 2 r.f. electrodes

Let us first consider structures consisting of rod d.c. electrodes a distance p above and below the plane containing the r.f. electrodes. This "sandwich" arrangement is shown in figure 3 a). It is based on construction (E) of section 4.2. All the d.c. electrodes are at the

same voltage.

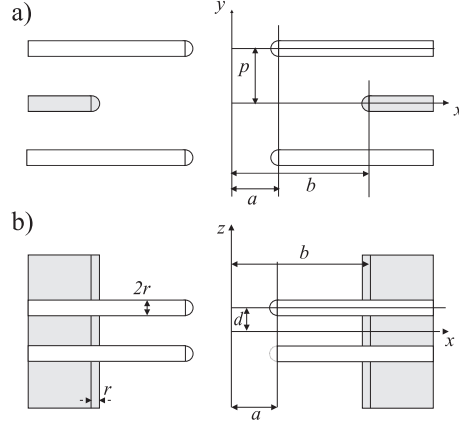


Fig. 3. Views of the electrode structure with 4 d.c. electrodes in two planes, and 2 r.f. electrodes. a) cross-section in the $x - y$ plane showing the sandwich structure. The r.f. electrodes are filled grey. b) View looking down on the $x - z$ plane from above.

Plan views of the two d.c. electrode structures tried are shown in figures 3b and 4. We let a set the overall distance scale, and then there are 4 parameters (b, d, p, r) and 2 constraints. The octopole configuration was found by fixing r and b , and then adjusting p and d .

The equipotential along the r.f. electrodes tends to prevent an octopole being produced at the origin. We found that it was necessary to restrict the influence of this equipotential by keeping p small. Since p must be larger than the electrode diameter this means that r must not be too large.

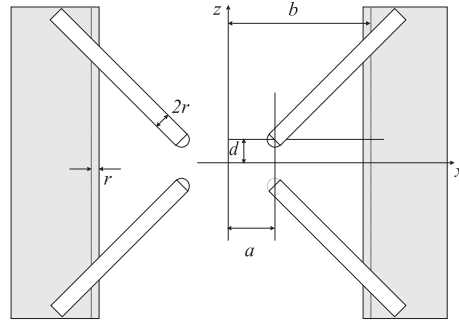


Fig. 4. A view of the electrode structure with 45 degree rod electrodes having hemispherical ends centred at $(\pm a, \pm b, \pm d)$. The r.f. electrodes have thickness $2r$, and lie in the $y = 0$ plane. The end of these electrodes are hemicylinders of radius r and centered on $x = \pm b, y = 0$. The grey fill represents the r.f. electrodes.

Results of the calculations for both structures are presented in table 1. The two cases produce similar values of γ and μ , those (labelled 1.1) for the structure shown in fig. 3b being somewhat higher than those (labelled 1.3) for the structure shown in fig. 4. It was found that the r.f. electrodes had to be placed well back (a large value for b) in order to get a high value

for γ .

Results 1.1 and 1.2 show that the value of μ decreases as b is reduced. This is because p and d also decrease, with the result that the influence of the r.f. electrodes is screened by the d.c. electrodes.

The geometry shown in figure 3 provides greater screening of the r.f. electrode by the d.c. electrodes, compared to that shown in figure 4, and this is probably the main reason why it provides the higher γ .

Table 1. Values of the distance parameters r, b, p, d which give an octopole for three example electrode structures, with the distance to an electrode surface ρ and the calculated geometric factors γ and μ in each case. Results 1.1 and 1.2 are for electrode configurations of the form shown in figure 3. Result 1.3 is for an electrode configuration like that shown in figure 4.

Result	r	b	p	d	ρ	γ	μ_x	μ_y
units	(a)	(a)	(a)	(a)	(a)	10^{-3}	10^{-3}	10^{-3}
1.1	0.30	6.30	1.94	2.01	2.67	26	6.40	6.45
1.2	0.37	3.34	1.16	1.28	1.63	18	3.44	3.77
1.3	0.26	4.95	1.20	0.88	1.53	15	4.80	3.14

5.2 10 d.c. electrodes in a plane, 4 r.f. electrodes

This structure consists of 10 d.c. electrodes in the $y = 0$ plane, and 4 r.f. electrodes in two planes parallel to this. It has reflection symmetry in $x - y$, $x - z$ and $y - z$ planes. The d.c. electrodes are cylindrical, with hemispherical ends centred at $x = \pm a$. Figure 5 shows a cross section in the $x - z$ plane for positive x .

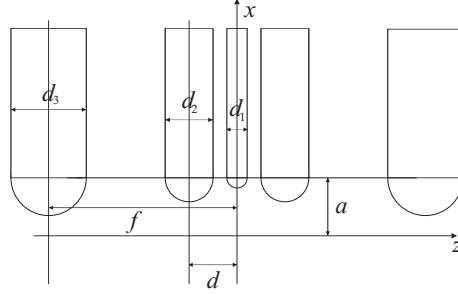


Fig. 5. 10 d.c. electrodes, 2 r.f. electrodes: A cross section view of the d.c. electrodes in the $x - z$ plane with $y = 0$ for positive x . The trap centre is at the intersection of the x and z axes. The electrode structure is repeated for negative x by reflection in the $z - y$ plane.

Each r.f. electrode is effectively a semi-infinite plane, with its edge parallel to the z axis. The y position of the r.f. electrodes is $\pm p$, and the x -position is $\pm(a + t)$, hence t gives the retraction of the r.f. electrodes. Where $p = 1.03$ the r.f. electrode had thickness $a/4$, otherwise the thickness was negligible. For the finite thickness cases, the edge of the electrode is hemicylindrical, and p and t give the position of the axis of the hemicylinder. An electrode structure with $p = 1.03a$ and $t = a$ is illustrated in figure 6.

The voltage on electrode 3 (V_3) was set to 1.4V in all the calculations in this section. With a fixed geometry our free parameters are the voltages on electrodes 1 and 2 (V_1 and V_2 respectively). These were adjusted to fulfill the octopole condition, using a two-dimensional

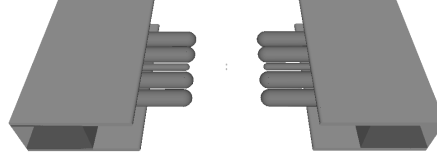


Fig. 6. A perspective view of the electrodes for r.f. electrodes positioned at $p = 1.03a$ and $t = a$. The 10 cylindrical electrodes have d.c. voltages applied to them. r.f. voltages are applied to the planar electrodes. Also shown are insulating spacers which hold the electrodes in place.

Newton-Raphson method in order to find the solution with few trials. Then the values of β , E_{\max} and γ were calculated. Adjustments were then made to f , d and d_3 , and the calculation repeated. A selection of positions and their corresponding values of γ are shown in table 2. The nearest electrode surface distance $\rho = 0.825a$ in all cases.

The initial choice of electrode diameters was $d_1 = 0.35a$, $d_2 = 0.825a$, $d_3 = 1.3a$, based on the indications from our initial line charge calculations. Using these diameters, CPO calculations were carried out with no r.f. electrodes for several values of f and d . The optimal values were found to be $f = 3.25a$ and $d = 0.825a$.

We then introduced the r.f. electrodes. With the r.f. electrodes far away from the d.c. electrodes ($p = 2a$ and $4a$) the maximum field is found between the d.c. electrodes, hence varying f makes little difference to the value of γ . This is because an increase (decrease) in β is countered by an increase (decrease) in E_{\max} . Cases 2.1 and 2.2 in table 2 illustrate this. For large d , the maximum field is found between electrodes 2 and 3, hence as d is reduced, E_{\max} decreases. For small d , the maximum field is found between electrodes 1 and 2, and then as d is reduced, E_{\max} increases. This behaviour is shown in figure 7.

Table 2. Results from CPO calculations. The simulations differ through values of f , d_3 , p and t . Results 2.1-2.6 are for the structures described in section 5.2, results 3.1-3.3 are for the structures described in section 5.3. For all of these cases, $d = 0.825a$, $d_1 = 0.35a$, $d_2 = 0.825a$, $V_{rf} = 0$ and $V_3 = 1.4V$.

Result	f	d_3	p	t	V_1	V_2	$10^4\beta$	E_{\max}	γ	μ_x	μ_y
	(a)	(a)	(a)	(a)	(V)	(V)	(V/a^4)	(V/a)	10^{-3}		
2.1	3.25	0.65	2	1	0.4605	0.2156	816	1.7	27	0.121	0.148
2.2	2.513	0.65	2	1	0.6657	0.2501	1421	2.6	31	0.111	0.147
2.3	3.25	0.413	4	3	0.6392	0.5065	500	1.9	14	0.096	0.110
2.4	3.25	0.65	1.03	0	0.0973	-0.0407	519	9	3.3	0.053	0.068
2.5	3.25	0.65	1.03	1	0.3085	0.0650	764	9	4.8	0.030	0.037
2.6	1.9	0.413	1.03	1	0.5218	-0.0055	1819	5	20	0.053	0.069
3.1	3.25	0.65	2	1	6.183	-1.207	506	55	5.0	0.150	0.152
3.2	3.25	0.65	1	1	0.3936	-0.2378	1387	15	6.2	0.046	0.043
3.3	3.25	0.65	2	3	4.969	-0.3090	86	32	10	0.027	0.030

When the r.f. electrodes are close to the d.c. electrodes ($p = 1.03a$), the maximum field is found between the d.c. electrode 3 and the r.f. electrodes. This field can be reduced by reducing d_3 . β increases as f is reduced, hence γ can also be increased by reducing f until the maximum field is found between the d.c. electrodes. Figure 8 shows this behaviour for structures with $p = 1.03a$ and $t = 0$.

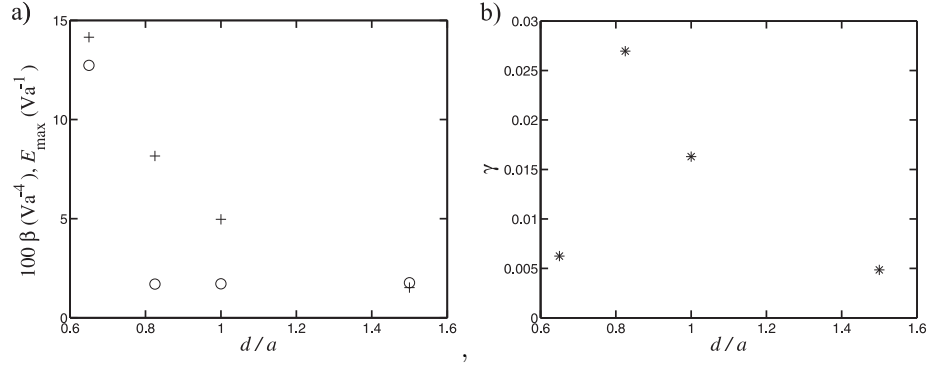


Fig. 7. The effect on β , E_{\max} and γ of adjusting d for result 2.1 in table 2. 100β is represented by +, and E_{\max} by unfilled circles. If the largest field lies between the first and second electrodes, then reducing d increases both β and E_{\max} , and γ drops. Where this is not the case, the increase in β causes an increase in γ .

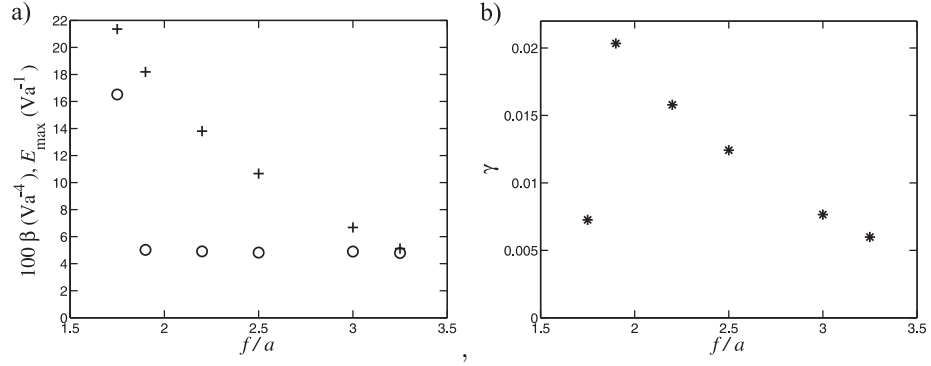


Fig. 8. The effect on β , E_{\max} and γ of adjusting f , with $d = 0.825a$, $d_1 = 0.35a$, $d_2 = 0.825a$, $d_3 = 0.825a$ and r.f. electrodes at $p = 1.03a$ and $t = 0$. 100β is represented by +, and E_{\max} by unfilled circles. Reducing f has the effect of increasing β . At larger f , the maximum field is found between the r.f. electrodes and the d.c. electrodes, hence we can increase γ by decreasing f . After reaching the point where the largest field is found between the d.c. electrodes, γ is much reduced for further reduction of f .

We also examined the effect of making electrode 3 extend further along the z direction. It was replaced by a planar electrode of thickness d_3 with edges rounded off by hemicylinders, located such that the edge nearest the origin was situated at the same place as the cylindrical electrode in the other results. This had little effect on γ or μ .

Finally, we examined an example in which the d.c. electrodes are extended along the z direction into planar shapes. This will reduce γ , but it also reduces the z -dependence of the a.c. part of the potential, therefore giving less micromotion along z . Each electrode had two flat surfaces parallel to the $x - z$ plane, and sides in the shape of hemicylinders having the same radius of curvature as before. The electrode centres were placed as in result 2.6 and they were extended along the z direction until the gaps between them were $0.1a$. This arrangement gave $\gamma = 2 \times 10^{-3}$, i.e. a factor 10 reduction compared to result 2.6.

5.3 20 d.c. electrodes in two planes, 2 r.f. electrodes

This arrangement is like the previous one, but with the d.c. and r.f. electrode positions swapped. It consists of 2 planar r.f. electrodes of thickness $0.5a$ lying in the $y = 0$ plane. These are bounded by hemicylindrical edges centred at $x = \pm(a + t)$. The d.c. electrodes lie in two planes at $y = \pm p$, each containing two sets of five d.c. electrodes (with f , d and electrode diameters the same as result 2.1 in table 2). Results for these arrangements are shown in table 2 as results 3.1-3.3. The values of γ and μ are similar to those in section 5.2. Some improvement in γ would be expected through optimisation of the relative positions of the d.c. electrodes. This has not been carried out in obtaining results 3.1-3.3.

5.4 Low Aspect Ratio Electrode Configurations

Let w be the total thickness, i.e. depth in y , of the electrode structure (c.f. figure 9). We define the aspect ratio $g = w/\rho$. The three-layer trap designs considered in sections 5.1, 5.2 and 5.3 have $g > 1$. Though microfabrication techniques are available which could be used to construct traps with $\rho \leq 100 \mu\text{m}$ and $g > 1$ [20], many methods are limited to a maximum structure thickness of around $20\mu\text{m}$ [11, 21]. This means that traps may have a low aspect ratio, $g < 1$.

We studied structures similar to those of section 5.2, but now with $g < 1$. To speed the calculation process we used cuboid shapes for the electrodes (see figures 9 and 10). The d.c. electrodes had width in z of $d_1 = d_2 = d_3 = w$, and were separated by gaps of $w/2$ (hence $d = 3w/2$, $f = 3w$). The thickness of the electrodes in y was $w/5$. With a cuboid shape the electric field diverges near the electrode edges. In order to calculate γ and μ we need to make some reasonable assumption to handle this. Our aim was to use the calculation to indicate approximately what would happen if in fact the electrode edges were smoothed. To this end we calculated electric field values at $(x, y, z) = (\rho, 0, 0)$, $(\rho + w/5, 0, d_1/2)$, $(\rho + t + w/5, w/10, 0)$ and at similar places around the other electrodes, and took E_{max} to be the largest of these.

Results for structures with $g = 0.4$ and $g = 0.2$ are shown in figure 11. We found that retracting the r.f. electrodes (i.e. using $t > 0$) gave a useful increase in both γ and μ . As the aspect ratio decreases, γ falls rapidly (and μ less rapidly).

5.5 Two-Layer Electrode Structures.

The most natural configuration for producing a radial r.f. quadrupole in the $x - y$ plane consists of electrodes placed at four corners of a square. Equal r.f. voltages are applied

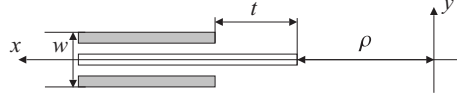


Fig. 9. A cross-section view of a low aspect ratio electrode structure for positive x showing the definition of the parameters w and t . The r.f. electrodes are represented by grey fill. The electrodes for negative x are obtained by a reflection in the $x = 0$ plane.



Fig. 10. Perspective view of a low aspect ratio electrode structure with $g = 0.4$ and $t/\rho = 0.6$.

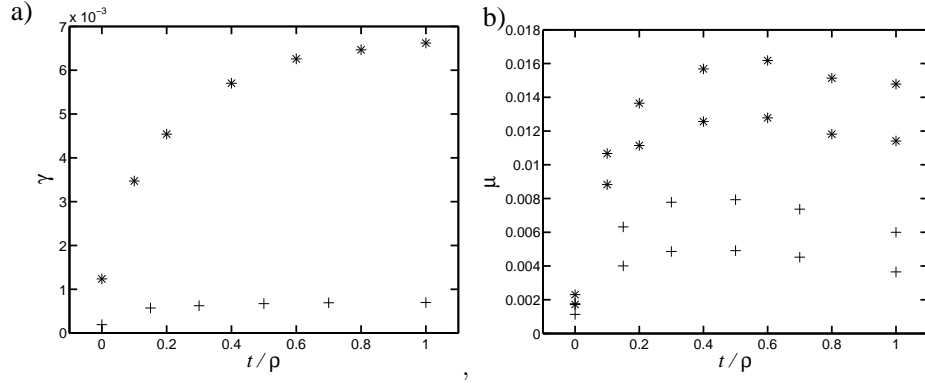


Fig. 11. Values of a) γ , b) μ for low aspect-ratio traps, as a function of the distance the r.f. electrodes are retracted with respect to the d.c. electrodes. Values for $g = 0.4$ structures are marked by *, and values for $g = 0.2$ are marked with a +. For a given g , the lower values of μ are μ_y , the upper values are μ_x .

to diagonally opposite electrodes. To produce an octopole by such an arrangement, one or more of these electrodes must be segmented. Choosing the structure to have 2-fold rotational symmetry about the z -axis, and reflection symmetry in the plane $z = 0$, there remain 3 constraints. We chose to satisfy the constraints by adjusting voltages rather than by accurately placing electrodes, and therefore two diagonally opposite electrodes must be split into seven segments.

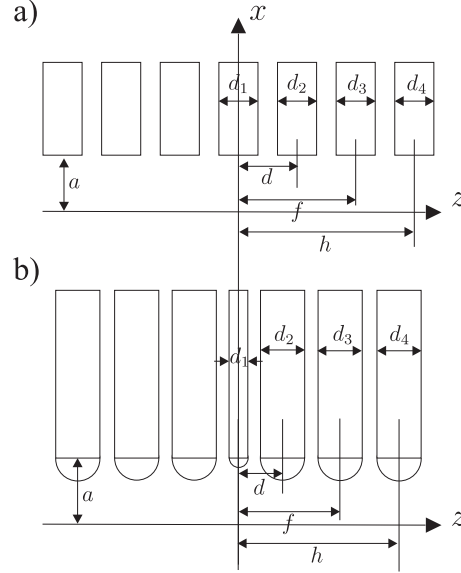


Fig. 12. The segmentation of the d.c. electrodes used in the two-layer electrode structures for a) cuboid electrodes and b) cylindrical electrodes. For cases where cuboidal electrodes were used, the electrode widths d_1 to d_4 were equal, and the separation between electrodes was $d_1/2$. For structures with cylindrical electrodes, $d_2 = d_3 = d_4 = 2.36d_1$.

The d.c. electrode segmentations used in the results presented below are shown in figure 12. The cuboid electrode structures consist of electrodes of equal width ($d_1 = d_2 = d_3 = d_4$), equally spaced by $d_1/2$ (hence $d = 3/2d_1$, $f = 3d$ and $h = 9/2d$). The cylindrical electrode structures were made up of cylinders parallel to the x axis with hemispherical ends. The diameters of the cylinders were $d_2 = d_3 = d_4 = 2.36d_1$. The axes of the cylinders were positioned at $d = 2.36d_1$, $f = 5.43d_1$ and $h = 8.43d_1$. The hemispherical ends of the cylinders were centred on $x = a$.

The r.f. electrodes consist of extended planes of thickness w_{rf} . For structures with cuboid electrodes, the end of the r.f. electrodes were placed at $x = \pm(a + t)$. For structures with cylindrical d.c. electrodes, the r.f. electrodes had hemicylindrical ends of radius $w_{rf}/2$ with axes parallel to the z axis at $x = \pm(a + t)$.

The voltage on d.c. electrode 4 was set to 1.4V, and the r.f. electrode voltage was set to 0V. Numerical calculations were performed for a range of values of d_1 , t and g , as defined in figures 12 and 13. Example results of these calculations are presented in table 3.

We found that the width d_1 of the central electrode had a strong effect on γ and a smaller effect on μ (see figure 14 and c.f results $\{4.5, 4.6\}$, $\{4.9, 4.10\}$). The optimum value of d_1 for

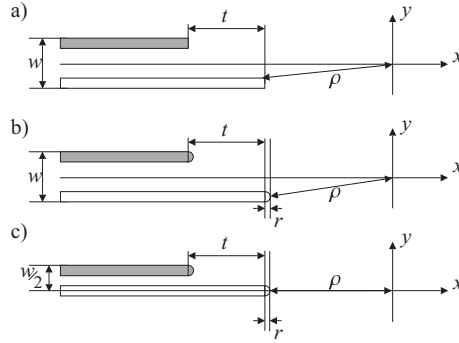


Fig. 13. Profiles of the two-layer electrode structures for negative x viewed in the $x-y$ plane. The r.f. electrodes are represented by grey fill. a) is the structure used to obtain results 4.1 to 4.12 in table 3, b) was used for results 4.13 to 4.15, and c) for results 4.16 and 4.17. The aspect-ratio of the trap was defined by $g = w/\rho$. The structure is repeated for positive x by a rotation of 180° about the z axis.

producing a d.c. octopole was found to be around 0.4ρ , for all values of g . This is comparable with the value used for the three layer electrode structures in section 5.2, which was obtained by examining the equipotentials of line-charge calculations. The monotonic increase in μ with d_1 may be ascribed to an increased influence of all of the d.c. electrodes.

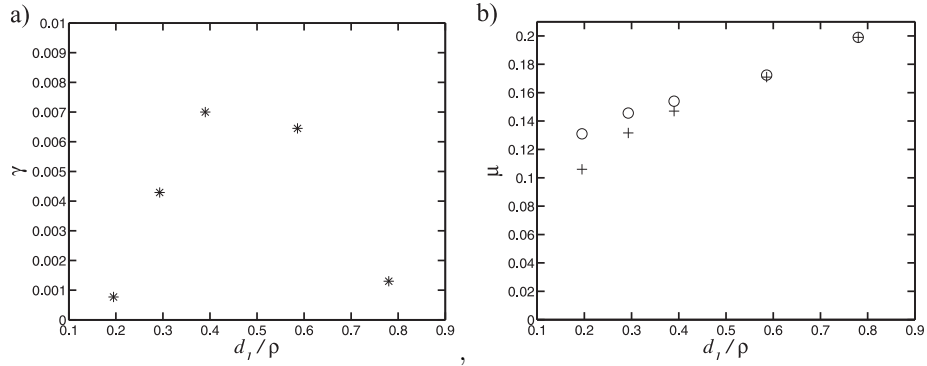


Fig. 14. The effect on a) γ and b) μ of adjusting the width of the central electrode for a two-layer electrode structure having $g = 2$ and $t = 0$. $\mu_{x'}$ is represented by unfilled circles and $\mu_{y'}$ by +.

Figure 15 shows the effect on γ and μ of changing the aspect ratio of the trap. For $g < 1$, both parameters increase with g . At higher g , μ continues to increase with g while γ decreases, presumably due to the reduced shielding of the r.f. electrodes by the d.c. electrodes.

We found that, for $g = 2$, retraction of the r.f. electrodes had no significant effect on γ , but reduced μ somewhat (results {4.1–4.3}). When $g = 0.4$ retraction allows a small increase in γ with a drop in μ (results 4.7,4.8). When $g = 0.24$, increasing t from 0 to $\rho/2$ increased γ by 40% with little effect on μ (results 4.10,4.11).

We examined the structure shown in figure 13, with the d.c. electrodes placed in the $y = 0$ plane, with a view to finding out whether it would produce a higher γ . However, comparison

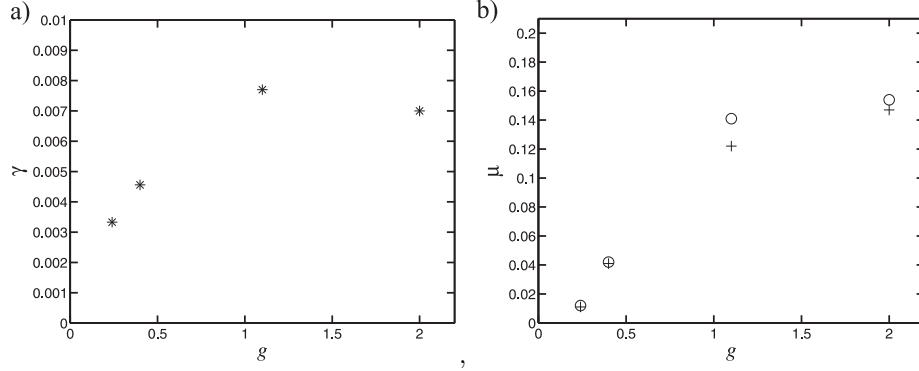


Fig. 15. The effect on a) γ and b) μ of adjusting the aspect ratio $g = w/\rho$ for a two layer electrode structure. In b), the values of μ plotted are those along the x' (represented by +) and y' (represented by o) axes of the quadrupole. The values of d_1 for these cases are similar but not identical (0.39, 0.47, 0.4 and 0.4 ρ from left to right on the plots).

of results 4.17 and 4.15 suggest that it has the reverse effect. Since μ decreases also there is nothing to be gained by adopting this structure.

5.6 Planar or near-planar arrangements

We considered cases where all the electrodes of the twin-trap system lie in a single plane (figure 16), and a simple ‘railway track’ arrangement in which rod-shaped r.f. electrodes run orthogonal to a set of simple rod-shaped d.c. electrodes (figure 17). The simplicity of such designs gives obvious advantages from the point of view of microfabrication, but we find that the penalty in terms of reduced factors γ and μ is severe. These results are presented in table 4.

The voltages on these structures are to be adjusted to produce a trapping region centred outside the electrode structure. Therefore they lack one reflection symmetry, and there are 6 constraints if we require an octopole (construction (G) of section 4.2). To satisfy all these constraints by adjusting voltages would require 7 d.c. voltages (in addition to the d.c. ground set by the r.f. electrodes) and therefore a large number of electrodes. In order to reduce the number of electrodes, we chose to examine structures such that the hexupole moment may be small but non-zero. We adjusted the 5 voltages labelled A–E in figures 16 and 17 so as to cancel the quadrupole terms and V_y and V_{yyy} , but we did not constrain V_{xxy} or V_{zzy} .

To find the condition where the d.c. hexupole/octopole is centred at the same height as the r.f. quadrupole, we proceeded as follows. First the r.f. electrodes were set to zero, and the d.c. voltages were adjusted to produce a hexupole/octopole at a few different heights. Next, the r.f. electrodes were allowed to go to ± 1 and the quadrupole position identified. We could then make a good first guess of the right d.c. voltages to get the desired coincidence, and the solution was found iteratively.

6 Discussion

A summary of the values of γ and μ obtained for the various structures we have considered is given in figure 18. We find that γ is always smaller than μ , and usually much smaller. This

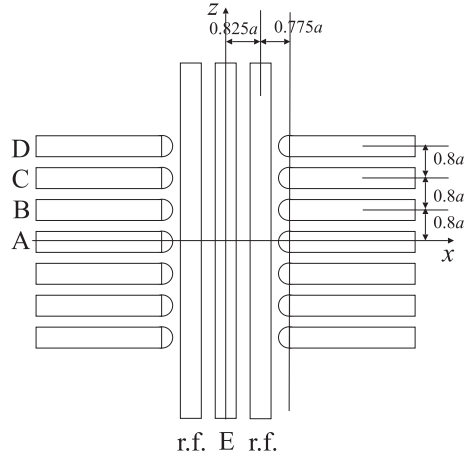


Fig. 16. The planar electrode arrangement (result 5.1). The cylindrical electrodes all lie in the same plane and have the same radius of $0.3a$. The ends of the electrodes parallel to the x axis are hemispherical.

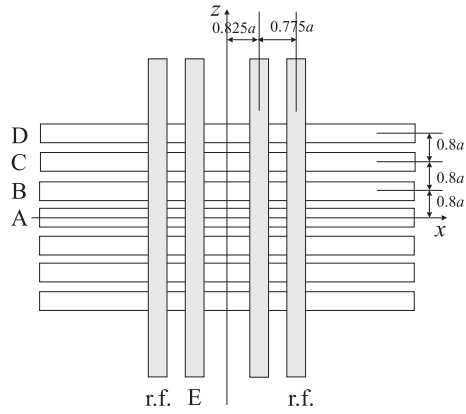


Fig. 17. Railway track electrode arrangement (result 5.2). The electrodes parallel to the z axis are situated above those parallel to the x axis by a distance of a . All electrodes are cylindrical, of radius $0.3a$.

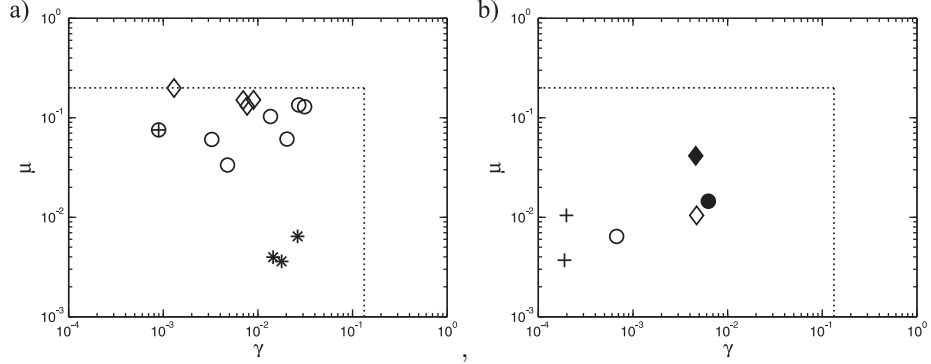


Fig. 18. Values of γ and μ for the structures considered in the text. (a): high aspect ratio, $g \geq 1$; *: 1.1–1.3, \circ : 2.1–2.6, \oplus : 3.1, \diamond : 4.1, 4.2, 4.7, 4.14. (b): low aspect ratio, $g \leq 0.75$; \circ : 3-layer, \diamond : 2-layer, $+$: ‘planar’ 5.1, 5.2 ($g \simeq 0.65$). The filled symbols represent results for $g \simeq 0.4$, the open symbols represent results for $g \simeq 0.2$. The dotted lines give the values which were obtained for the two ‘standard’ cases described in section 5, for comparison.

may be because we have not allowed the r.f. electrode to be divided. It presents a flat potential surface along the z direction which tends to suppress the variation in potential which is needed for large γ . It may be possible to increase γ without introducing multiple r.f. electrodes, by tailoring the shape of the edge of the r.f. electrodes to follow an equipotential produced by the d.c. octopole.

One might expect a competition between μ and γ to be observed in the results, but there is little indication of this. The best structures give high γ and high μ simultaneously.

Many of the optimizations studied, by adjusting the widths and placements of electrodes, gave useful improvements in γ and/or μ . This implies that a careful optimization of any chosen design is worthwhile.

Of the three-layer electrode structures we examined, those of the general form shown in figure 6 performed best. The highest γ value ($\gamma \simeq 0.03$, result 2.2), was obtained with μ close to the highest value, using a 3-layer structure of aspect ratio $g \simeq 3$.

At lower aspect ratio, $g < 0.5$, the two-layer structures performed better than three-layer ones of the same g (figure 18b). The larger value for γ may be understood from the fact that when g is small, γ varies rapidly with w because thicker electrodes can extend their influence on $V(x, y, z)$ over larger distances. For a given total depth w of the whole structure, if there are m layers and $m - 1$ gaps all of the same thickness, then the thickness of each layer is $w/(2m - 1)$. Therefore a two-layer structure of given g may be expected to give a similar value for γ as a three-layer structure with g larger by a factor $5/3$. This may be seen by comparing the values for a three-layer structure at $g = 0.4$ in figure 11 with those for a two-layer structure at $g = 0.24$, e.g. result 4.11 (and c.f. figure 18b). The two-layer structures also give larger values for μ at given g . This is in part for a similar reason, and also because the electrodes are more conveniently placed to realise a radial quadrupole.

At $g = 0.24$ the highest γ value ($\gamma \simeq 0.005$, result 4.11) was smaller than the best overall by a factor 6, and μ was reduced by an order of magnitude.

The planar or near-planar arrangements, cases 5.1 and 5.2, gave a further order of mag-

nitude reduction in γ compared to the two-layer low-aspect-ratio structure.

7 Conclusions

We have studied the general problem of separating or bringing together pairs of trapped ions, while keeping the frequencies of the normal modes of oscillation of the ions as high as possible. A simple picture of this is to say the central electrode introduces a potential hill which pushes the ions apart. However we found that the distance between the ions can be small compared to the distance scale of the electrodes, even when the potential well is about to divide into two local minima. This means that the potential shape in the region between the ions is really a joint property of the whole set of electrodes. There are various contributions to the potential that have a quadratic dependence on position near the origin, and when the ions are being split or recombined these are balanced, so as to leave a quartic dependence. We did not study the degree of precision in the control voltages that is needed to maintain this balance. It would be advisable to study this issue before finalising any trap design.

We found that the problem under consideration has a natural length scale L_0 (equation (22)), set by the maximum electric field allowed in the structure. Since this varies as $E_{\max}^{1/2}$ it will not change greatly for different materials or fabrication methods, and values in the region a few nm to some tens of nm are to be expected. If the trap structures are large compared to $\rho_c \simeq 100L_0$, then, roughly speaking, producing the d.c. octopole is more demanding than producing the r.f. quadrupole. Ion trap micro-fabrication methods being attempted at present are in the regime $\rho \gg \rho_c$.^a

Overall, our results suggest that it is worthwhile to fabricate structures which require two or more layers. We found that for large aspect ratio g , 3-layer designs performed best, while at low aspect ratio, 2-layer designs performed best at a given value of g . Current efforts to fabricate trap arrays are focussed on distances of order $\rho \simeq 100 \mu\text{m}$ and this suggests a low aspect ratio $g \simeq 0.2$ will be necessary if lithographic methods are used. In the future, however, there may be interest in $\rho \simeq 10 \mu\text{m}$ and then $g \simeq 2$ may be available.

It is not surprising that the 3-layer designs offer tighter traps than the planar designs, but it is noteworthy that when considering the problem of separating ions, this is especially true. The factor $\simeq 150$ decrease in γ (comparing case 2.2 in table 2 with case 5.1 in table 4) means that the planar design would need to be fabricated at a distance scale a factor $150^{1/3} \simeq 5$ times smaller in order to obtain the same motional frequency ω_1 (equation (19)). If we assume heating rates scaling as ρ^{-4} , the heating rate in the latter case would be increased compared to the former by a factor $\simeq 800$.

It should be noted that our whole study has ignored any possible heating or control problems associated with micromotion. The structures we have studied produce an oscillating contribution to $V(x, y, z)$ that is mostly but not purely a two-dimensional quadrupole in the radial direction. That is to say, there is some z -dependence in the oscillating part of the potential, and therefore micro-motion along the z axis. Further studies would be needed to discover the influence of micro-motion on the dynamics of a pair of ions as they are separated or brought together. To reduce micro-motion, one may require electrode surfaces to be parallel

^aMethods have been suggested to approach the nanometre scale, such as the use of carbon nanotubes as electrodes. The use of very tight traps would require novel non-optical methods to achieve quantum logic gates, because the Lamb-Dicke parameter would be very small.

to the z axis where possible.

Acknowledgements

We thank D.N.Stacey, M.G.Blain and J.Fleming for helpful discussions

This work was supported by the EPSRC, the Research Training and Development and Human Potential Programs of the European Union, the National Security Agency (NSA) and Advanced Research and Development Activity (ARDA) (P-43513-PH-QCO-02107-1).

References

1. C. A. Sackett, D. Kielpinski, B. E. King, C. Langer, V. Meyer, C. J. Myatt, M. Rowe, Q. A. Turchette, W. M. Itano, D. J. Wineland, and C. Monroe. Experimental entanglement of four particles. *Nature*, 404:256–258, March 2000.
2. M. Riebe, H. Hffner, C. F. Roos, W. Hnsel, J. Benhelm, G. P. T. Lancaster, T. W. Krber, C. Becher, F. Schmidt-Kaler, D. F. V. James, and R. Blatt. Deterministic quantum teleportation with atoms. *Nature*, 429:734–737, 2004.
3. C. F. Roos, M. Riebe, H. Haffner, W. Hansel, J. Benhelm, G. P. T. Lancaster, C. Becher, F. Schmidt-Kaler, and R. Blatt. Control and measurement of three-qubit entangled states. *Science*, 304(1478), 2004.
4. D. Kielpinski, C.Monroe, and D. Wineland. Architecture for a large-scale ion-trap quantum computer. *Nature*, 417:709–711, June 2002.
5. D. J. Wineland, C. Monroe, W. M. Itano, D. Leibfried, B. E. King, and D. M. Meekhof. Experimental issues in coherent quantum-state manipulation of trapped atomic ions. *J. Res. Natl. Inst. Stand. Technol.*, 103:259–328, 1998.
6. A. M. Steane. Quantum computer architecture for fast entropy extraction. *Quant. Inf. and Comp.*, 2:297–306, 2002. quant-ph/0203047.
7. M. A. Rowe, A. Ben-Kish, B. DeMarco, D. Leibfried, V. Meyer, J. Beall, J. Britton, J. Hughes, W. M. Itano, B. Jelenković, C. Langer, T. Rosenband, and D. J. Wineland. Transport of quantum states and separation of ions in a dual rf ion trap. *Quantum Information and Computation*, 2(4):257, 2002.
8. M. D. Barrett, J. Chiaverini, T. Schaetz, J. Britton, W. M. Itano and J. D. Jost, E. Knill, C. Langer, D. Leibfried, R. Ozeri, and D. J. Wineland. Deterministic quantum teleportation of atomic qubits. *Nature*, 429:737–739, 2004.
9. Q. A. Turchette, D. Kielpinski, B. E. King, D. Leibfried, D. M. Meekhof, C. J. Myatt, M. A. Rowe, C. A. Sackett, C. S. Wood, W. M. Itano, C. Monroe, and D. J. Wineland. Heating of trapped ions from the quantum ground state. *Phys. Rev.*, A61:063418, 2000.
10. L. Deslauriers, P. C. Haljan, P. J. Lee, K.-A. Brickman, B. B. Blinov, M. J. Madsen, and C. Monroe. Zero-point cooling and low heating of trapped cd ions. *Phys. Rev. A*, 2004. quant-ph/0404142.
11. M. J. Madsen, W. K. Hensinger, D. Stick, J. A. Rabchuk, and C. Monroe. Planar ion trap geometry for microfabrication. *Appl. Phys. B*, 78:639–651, 2004.
12. M. Šašura and A. M. Steane. Fast quantum logic by selective displacement of trapped ions. *Phys. Rev.*, A67(062318), 2003.
13. A. Sørensen and K. Mølmer. Entanglement and quantum computation with ions in thermal motion. *Phys. Rev.*, A62(022311), July 2000.
14. H. G. Dehmelt. Radiofrequency spectroscopy of stored ions. *Adv. At. Mol. Phys.*, 3(53), 1967.
15. Prahdip K. Ghosh. *Ion Traps*. Clarendon Press, Oxford, 1995.
16. D. Cruz, J.P. Chang, and M. G. Blain. Field emission characteristics of a tungsten micro-electrical mechanical system device. *preprint*, ., 2004.
17. R. Gomer. *Field Emission and Field Ionization*. Harvard University Press, Cambridge, 1961.
18. Idaho National Engineering and Environmental Laboratory. Simion 3d version 7.0, 2000.

19. CPO Ltd. Charged particle optics programs.
20. J.R. Reid and R.T. Webster. A 60 ghz branch line coupler fabricated using integrated rectangular coaxial lines. *IEEE*, 2004.
21. M. G. Blain, L. S. Riter, D. Cruz, D. E. Austin, G. Wu, W. R. Plass, and R. Graham Cooks. Towards the hand-held mass spectrometer: design considerations, simulation, and fabrication of micrometer-scaled cylindrical ion traps. *International Journal of Mass Spectrometry*, 236:91–104, 2004.

Appendix: Basic octopole constructions

We list some combinations of point and line charges that produce octopoles using a minimal number of separate points or lines.

7.1 Systems of point charges

8 point charges q at the corners of a regular cube of side $2a$ produce an octopole having cubic symmetry (25) with $\beta = 7q/81\sqrt{3}\pi\epsilon_0 a^5$.

If we search for a system of 8 point charges all lying in a single plane $y = 0$, the only solution is the one produced by the construction (27), (28). This is shown in figure 19a. In the positive quadrant there is a charge q at $(x, z) = (a, d)$ and a charge $-f^3 q$ at (fa, fd) . For example, $a = d$ gives $\beta = (-13q/128\sqrt{2}\pi\epsilon_0 a^5)(1 - 1/f^2)$; the coefficients of x^4, y^4 and z^4 are then in the ratios 13 : -12 : 13, and the potential is a combination of axial and 2D octopoles in the ratio -24 : 35. When $d = a/\sqrt{2}$ then each set of 4 charges on its own produces a potential with $\partial^2 V / \partial z^2(0, 0, 0) = 0$, and the two sets as described produce equal and opposite $\partial^2 V / \partial x^2(0, 0, 0)$. This gives $\beta = (-14\sqrt{2/3}q/81\pi\epsilon_0 a^5)(1 - 1/f^2)$; the coefficients of x^4, y^4 and z^4 are in the ratios 26 : -54 : 56. Similar remarks apply with x and z swapped when $d = \sqrt{2}a$.

7.2 Systems of ring and line charges

The potential produced by a semi-infinite straight line charge is $V = (\lambda/2\pi\epsilon_0) \ln(r + z)$, in a coordinate system such that the line charge lies on the negative z axis and ends at the origin ($r = (x^2 + y^2 + z^2)^{1/2}$).

An axially symmetric octopole (24) can be created by a single pair of identical ring charges on a common axis, whose separation is $\sqrt{2}$ times larger than their radius (shown in figure 19c). For charge per unit length λ and radius a , $\beta = -14\sqrt{2/3}\lambda/81\pi\epsilon_0 a^4$. This charge distribution can also be interpreted as a rotation about the z axis of point charges at the ‘special’ location $x = z/\sqrt{2}$ which we identified in the preceeding section.

Addition of a further pair of rings allows a solution at any values of the ring separations, by adjusting the free parameter of the relative charge per unit length.

A set of 8 identical line charges, ending at the corners of a regular cube of side $2a$, and extending outwards along the extended major diagonals, produces an octopole having cubic symmetry (25) with $\beta = -56\lambda/2592\pi\epsilon_0 a^4$, where λ is the charge per unit length.

Next let us consider two sets of 4 line charges lying in two parallel planes (construction (E) of section 4.1). To reduce the number of parameters, we consider semi-infinite lines. We take the origin at the centre of symmetry, and orient axes so that the two planes are parallel to the $x - z$ plane. Apart from an overall scale factor, there are then three parameters which describe the layout: the angular coordinates of the end of one of the lines, which may be

specified for example by spherical polar angles θ , ϕ , and the angle φ between the line charge and the z -direction. This is shown in figure 19d. Since we have three parameters (θ, ϕ, φ) and two constraints (30), one parameter may be chosen arbitrarily and the others adjusted to find a solution. For example in the construction (E) we pick φ and then adjust θ and ϕ . We will list some example solutions. For convenience, we specify θ, ϕ by giving the rectangular coordinates (x, y, z) of the end of the line lying in the positive octant, with an arbitrary scale factor. Example solutions are $(x, y, z, \varphi) = (1, 1, 0, 0)$, $(1, 1.434, 0.578, \pi/6)$, $(1, 1.799, 1, \pi/4)$, $(1, 2.482, 1.731, \pi/3)$, $(0, 1, 1, \pi/2)$.

A set of 4 parallel infinite line charges passing through the corners of a square in a plane perpendicular to them (figure 19e) produces a 2D octopole (26) with $\beta = \lambda/8\pi\epsilon_0 a^4$, where the square has side $2a$ (see figure 19e).

A set of 4 infinite line charges passing along the sides of a cube as in figure 19f produces an octopole having $\beta = -3\lambda/4\pi\epsilon_0 a^4$, at the centre of the cube, where the cube has side $2a$.

Next, consider sets of semi-infinite line charges all lying in a single plane. Let the plane be the $x - z$ plane and assume symmetry under reflections in the x and z axes. First suppose there is only a single line charge in the positive quadrant (so 4 line charges in total). The geometry has two parameters: the angle θ between the z axis and a vector from the origin to the end of the line, and the angle φ between the line itself and the z -direction. This suggests it might be possible to obtain $\partial^2 V/\partial x^2 = \partial^2 V/\partial z^2 = 0$ by a good choice of θ and φ , but the pair of simultaneous equations has no solution. The construction (D) (eq. (28)) leads to an infinite set of solutions with 8 electrodes in two groups of four. The two groups have the same values of θ and φ ; the charge per unit length on the outer group is greater than that on the inner group by a factor f^2 . There are further solutions when the two groups have different angles. As an example case, shown in figure 19b, $\theta = \pi/4$, $\varphi = \pi$ (line charges parallel to the x axis and finishing on the line $x = z$) gives $\beta = -(15\lambda(16 + 11\sqrt{2})/16\pi\epsilon_0(1 + \sqrt{2})^4 a^4)(1 - 1/f^2)$.

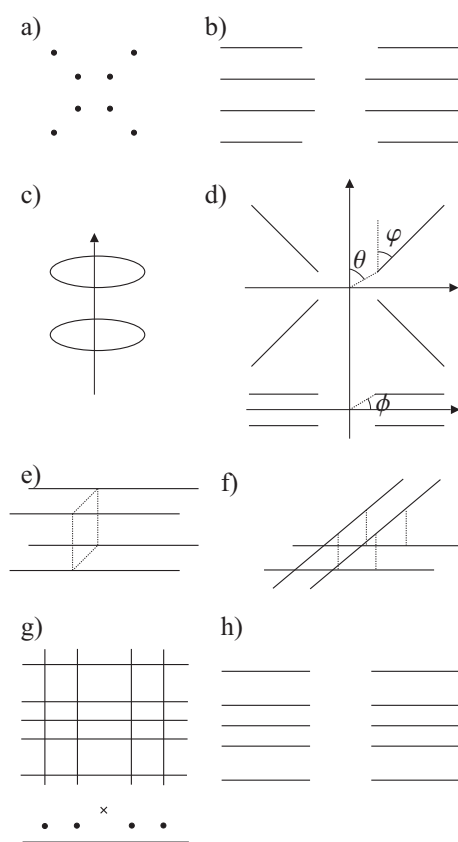


Fig. 19. Examples of octopole constructions using line charges.

Table 3. Results from numerical calculations for the two-layer electrode structures. The value of E_{\max}^{μ} was calculated using an r.f. electrode voltage of 10^6 V. Results 4.1 to 4.12 use cuboid electrodes. Results 4.13 to 4.17 use cylindrical d.c. electrodes in the arrangement shown in figure 12. 4.13 to 4.15 are for case (b) in figure 13, 4.16 and 4.17 for case (c) in figure 13.

Result units	g	w_{rf} (ρ)	d_1 (ρ)	t (ρ)	V_1 (V)	V_2 (V)	V_3 (V)	$10^4\beta$ (Va^{-4})	E_{\max} (Va^{-1})	γ (10^{-3})	E_{\max}^{μ} (10^6Va^{-1})	$\mu_{x'}$	$\mu_{y'}$
4.1	2	0.16	0.39	0	-1.8451	1.4055	-3.2924	-710	21	-7.0	1.77	0.147	0.154
4.2	2	0.16	0.39	0.39	-1.6997	2.2963	-3.1155	-728	23	-7.4	1.70	0.114	0.124
4.3	2	0.16	0.39	0.78	-1.8592	2.4805	-3.3316	-872	25	-7.5	1.53	0.097	0.109
4.4	2	0.16	0.78	0	-0.0885	0.3648	-1.6934	-131	7.8	-1.30	1.32	0.199	0.199
4.5	1.1	0.19	0.94	0	-0.0290	0.2095	-1.6090	-98	9	-1.3	2.25	0.122	0.158
4.6	1.1	0.19	0.47	0	-0.7951	1.4055	-2.5750	-1304	20	-7.7	2.42	0.122	0.141
4.7	0.4	0.08	0.40	0	-1.4109	2.0817	-3.1413	-1563	34	-4.6	4.37	0.041	0.042
4.8	0.4	0.08	0.40	0.5	-1.4960	2.1987	-3.0247	-1848	33	-5.5	4.59	0.028	0.031
4.9	0.24	0.08	0.20	0	-11.582	10.442	-6.3685	-1094	233	-0.47	12.6	0.007	0.011
4.10	0.24	0.08	0.40	0	-1.3316	1.9730	-3.0171	-1250	38	-3.3	12.7	0.011	0.012
4.11	0.24	0.08	0.40	0.5	-1.2679	1.8959	-2.7263	-1636	35	-4.7	12.8	0.0099	0.011
4.12	0.24	0.08	0.40	1	-1.1612	1.9083	-2.5576	-1649	34	-5.0	12.7	0.0061	0.0068
4.13	1.28	0.24	0.17	0	-22.030	4.7513	-4.5768	-399	229	-1.6	19.1	0.097	0.100
4.14	2.56	0.42	0.28	0.8	25.107	-5.2939	18.252	12724	257	8.5	16.8	0.120	0.112
4.15	2.56	0.42	0.4	0.4	-0.3793	0.1728	-1.3831	-482	9.2	-9.0	16.2	0.167	0.136
4.16	2.56	0.61	0.42	1.21	-0.1479	0.1103	-0.8449	-970	10	-5.4	36.5	0.030	0.041
4.17	2.56	0.61	0.42	0.4	-0.1427	0.0917	-0.7954	-885	10	-5.0	33.3	0.048	0.067

Table 4. The two cases studied which produced almost-octopoles above the plane of the electrodes. Result 5.1 uses the single plane electrode geometry shown in figure 16. Result 5.2 uses the “railway track” geometry shown in figure 17.

Result units	V_A (V)	V_B (V)	V_C (V)	V_E (mV)	$10^4\beta$ (V/a^4)	E_{\max} (V/a)	ρ (a)	γ (10^{-3})	μ_x (10^{-3})	μ_y (10^{-3})
5.1	-4.257	4.560	-3.527	-2.197	-0.0155	44.74	0.829	0.198	10.4	10.5
5.2	1.089	1.212	-4.526	-201	0.000247	20.47	2.5	0.189	3.5	3.9